Journal of Materials Chemistry A

Accepted Manuscript

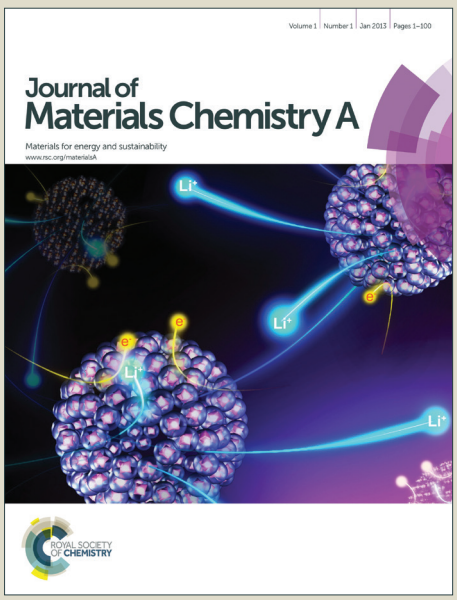

ROYAL SOCIETY OF CHEMISTRY

www.rsc.org/materialsA

Battery/Supercapacitor Hybrid via Non-Covalent Functionalization of Graphene Macro-Assemblies

P. G. Campbell*, M. D. Merrill, B. C. Wood, E. Montalvo, M. A. Worsley, T. F. Baumann, J. Biener

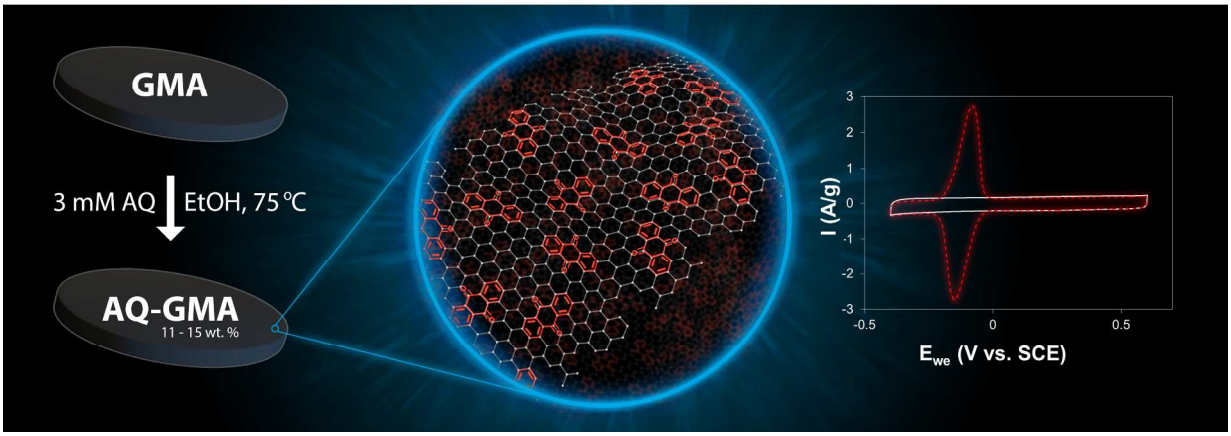

A 2.9-fold increase in electrical energy storage capacity (up to 23 Wh/kg) is achieved in battery/supercapacitor hybrid electrodes through non-covalent modification of binder-free, ultra-high surface area graphene macro-assemblies with redox-active anthraquinone. These hybrid electrodes demonstrate battery-like energy density combined with supercapacitor-like power performance and superb long-term cycling stability.

Keyword: porous materials, electrodes, supercapacitors, energy storage, graphene

Abstract: Binder-free, monolithic, high surface area graphene macro-assemblies (GMAs) are promising materials for supercapacitor electrodes, but, like all graphitic carbon based supercapacitor electrodes, still lack sufficient energy density for demanding practical applications. Here, we demonstrate that the energy storage capacity of GMAs can be increased nearly 3-fold (up to 23 Wh/kg) by facile, non-covalent surface modification with anthraquinone (AQ). AQ provides battery-like redox charge storage (927 C/g) without affecting the conductivity and capacitance of the GMA support. The resulting AQ-GMA battery/supercapacitor hybrid electrodes demonstrate excellent power performance, show remarkable long-term cycling stability and, by virtue of their excellent mechanical properties, allow for further increases in volumetric energy density by mechanical compression of the treated electrode. Our measured capacity is very close to the theoretical maximum obtained using detailed density functional theory calculations, suggesting nearly all incorporated AQ is made available for pseudocapacitive charge storage.

Journal of Materials Chemistry A RSCPublishing

PAPER

Battery/Supercapacitor Hybrid via Non-Covalent Functionalization of Graphene Macro-Assemblies

Cite this: DOI: 10.1039/xoxxoooooox

P. G. Campbell*, M. D. Merrill, B. C. Wood, E. Montalvo, M. A. Worsley, T. F. Baumann, J. Biener

Received ooth January 2012,
Accepted ooth January 2012

DOI: 10.1039/xoxxoooooox

www.rsc.org/

Binder-free, monolithic, high surface area graphene macro-assemblies (GMAs) are promising materials for supercapacitor electrodes, but, like all graphitic carbon based supercapacitor electrodes, still lack sufficient energy density for demanding practical applications. Here, we demonstrate that the energy storage capacity of GMAs can be increased nearly 3-fold (up to 23 Wh/kg) by facile, non-covalent surface modification with anthraquinone (AQ). AQ provides battery-like redox charge storage (927 C/g) without affecting the conductivity and capacitance of the GMA support. The resulting AQ-GMA battery/supercapacitor hybrid electrodes demonstrate excellent power performance, show remarkable long-term cycling stability and, by virtue of their excellent mechanical properties, allow for further increases in volumetric energy density by mechanical compression of the treated electrode. Our measured capacity is very close to the theoretical maximum obtained using detailed density functional theory calculations, suggesting nearly all incorporated AQ is made available for pseudocapacitive charge storage.

Introduction

In order to enable the widespread adoption of emission-free energy sources such as solar and wind for electricity generation, as well as free the transportation sector from dependence on fossil fuels, new technologies and materials for electric energy storage must be developed.[1] Energy storage systems for electric vehicles have especially demanding requirements as they must combine high power and energy density, cyclability, safety, and low cost. Here, supercapacitors (also known as ultracapacitors or electrical double-layer capacitors) can help to meet these requirements due to their high power density and excellent cycling stability.[1,2] Graphene-based supercapacitor electrodes are particularly promising because they feature high surface area, good electrical conductivity, and chemical inertness.[3,4] Using abundant and low cost starting materials, we recently developed binder-free 3D mesoporous graphene macro-assemblies (GMAs) that have exceptionally high surface area (up to 1500 m^2/g) and excellent conductivity (up to 100 S/m).[5-7] Compared to traditional carbon-based electrodes fabricated from carbon black and binder materials, GMAs offer many advantages such as deterministic control of density and pore size distribution and increased conductivity due to covalent sp^2 carbon linkers between the active carbon sheets and the absence of binder materials. However, for practical applications even these materials will require further improvements to their energy storage performance as the interfacial capacitance of graphitic carbon-based electrodes is fundamentally limited by the low density of states at the Fermi level to ~10 $\mu F/cm^2$ (corresponding to 0.01 electron per carbon atom for the stability window of aqueous electrolytes).[8-10] One strategy is to increase the *volumetric* energy density of GMAs by increasing the density of these highly porous materials through mechanical compression.[11] Here, we explore non-covalent surface functionalization with anthraquinone as a redox-active material to further improve the *gravimetric* energy density of GMAs.

The addition of redox active components promises more efficient charge storage by adding a pseudocapacitive and/or fast faradaic charge storage channel to the system.[12,13] The challenge, however, is to do this without deteriorating the main advantages of supercapacitor electrodes, which are excellent cycling stability and power performance. Integrating metal-oxide thin films or nanoparticles into porous electrodes has recently been investigated,[14,15] with particularly good performance reported for materials containing MnO_2,[16,17] V_2O_5,[18] and Nb_2O_5.[19] The main drawbacks of metal-oxide treated carbon electrodes are their limited stability upon cycling, and the relatively high cost, high weight, and potential negative environmental impact of metal oxides.

Redox active small organic molecules or polymers can provide additional charge storage capacity. Quinones have been

widely utilized for this application due to their low cost, high stability, and because their aqueous redox properties are well understood.[20] Quinone-based redox systems involve interfacial proton-coupled electron transfers, which are fast and therefore likely to facilitate greater power densities than other redox systems involving larger and slower Li^+ or OH^- ions. For example, 9,10-anthraquinone (AQ) stores 0.14 electron per carbon atom and has a formal potential of –0.1 V vs. SCE in acidic media, which is close to the cathodic limit of an aqueous acidic electrolyte (an important consideration, so that additional charge is provided at the beginning of supercapacitor discharge when voltage is high). A number of methods have been developed to covalently attach AQ to carbon electrodes, which can increase energy density by up to 86% over untreated electrode materials.[21-26] However, covalent modification to graphene-based electrodes disrupts the conductive sp^2 carbon network by local sp^2-to-sp^3 rehybridization and reduces the underlying double-layer capacitance of the electrode.

Non-covalent modification of graphene-based electrodes, on the other hand, avoids this problem by utilizing van der Waals interactions to anchor redox active components to the graphitic network. This approach does not disturb the conducting sp^2 carbon network and thus may not affect the power performance or the double-layer capacitance of graphene-based supercapacitor electrodes. Non-covalent modification also simplifies material preparation by reducing the number of steps and reagents required. Roldán *et al.* were able to significantly increase the capacitance of several carbon electrodes through the addition of hydroquinone to the electrolyte, but long-term stability proved to be a challenge with 65% of initial capacitance remaining after 4,000 cycles.[27] Wang *et al.* achieved good capacitance at high charge rates using reduced graphene oxide electrodes treated with more hydrophobic *t*Bu-hydroquinone, and maintained 94% of initial capacitance after 800 cycles (the extent of their measurement).[28] Quinone derivatives of polyaromatic hydrocarbons (PAHs), such as anthraquinone, are also more hydrophobic than hydroquinone/benzoquinone and have an extended π-electron system that can increase the strength of non-covalent attractions (e.g., through π-π stacking). Anjos *et al.* have evaluated the supercapacitor performance of various PAH-quinones adsorbed on onion-like carbons (OLCs) and reported excellent cycling stability; up to 97% of initial capacitance remained after 10,000 cycles though the performance of these devices is limited by the relatively low surface area of OLCs.[29,30] Very recently, Wang, Guo and coworkers reported a 2.3-fold improvement in capacitance by mixing anthraquinone with porous carbon nanotubes.[31]

Here, we report a method to increase the energy density of GMA electrodes to near battery levels while maintaining the excellent power and cycling performance of supercapacitors via facile, non-covalent functionalization with anthraquinone (referred to in the text as AQ-GMAs). The resulting battery/supercapacitor hybrid electrodes have 2.9 times the electrical energy storage capacity of untreated GMA electrodes without reduction in high-power performance and maintain at least twice the capacity of untreated GMA electrodes for 10,000 charge-discharge cycles. We also realized up to 8X increased volumetric energy density through mechanical compression of the treated electrode. This is made possible by the monolithic, binder free nature of the GMAs, which allows for very high strain values without mechanical failure. The experimental results are in excellent agreement with high-level density functional theory (DFT) calculations probing the theoretical maximum capacity of AQ-GMAs and their charge storage characteristics.

Results and discussion

Preparation of Anthraquinone-Coated GMAs (AQ-GMAs)

Disk-shaped graphene macro-assemblies were prepared in a similar manner to what has been previously reported by our group (for details, see the electronic supporting information, ESI).[6] The GMA disks used here are approximately 1 cm in diameter by 250 μm thickness, weigh ~1 mg, have a density of ~0.07 g/cm^3, and a BET surface area of ~1300 m^2/g. Non-covalent 9,10-anthraquinone (AQ) functionalization was achieved by soaking GMA disks in a 3 mM solution of AQ in EtOH for 2 h at 75 °C (**Figure 1a**). This reliably resulted in AQ loadings of 10-14 wt.% with respect to GMA mass, at the high end of reported loadings for covalently modified graphitic electrodes that range from 7.1 wt.%[21] – 14 wt.%.[25] Longer soaking times (up to 24 h) and increased AQ concentration (5 mM in EtOH) did not increase the AQ loading. Loading levels were determined by weighing samples before and after AQ treatment using a high-precision analytical microbalance (Mettler-Toledo XP2U). These measurements were confirmed by thermogravimtric analysis (TGA). The TGA curves for an 11.2 wt.% AQ-GMA sample, along with bulk AQ, are shown in **Figure 1b,c**. The derivatives of the mass loss curves show peaks at different temperatures for AQ-GMA and bulk AQ. The shift of the AQ-GMA peak by more than 60 °C towards higher temperature is a result of the adsorption of the AQ molecule on the carbon substrate[32] and indicates diffusion-limited desorption kinetics (the number of wall collisions necessary to diffuse from the interior of a monolithic nano-meso porous bulk sample to the sample surface scales with the square of the aspect ratio, and thus requires >10^6 wall collisions for the combination of sample thickness and pore size in GMA).[33,34]

Electrochemical Measurements

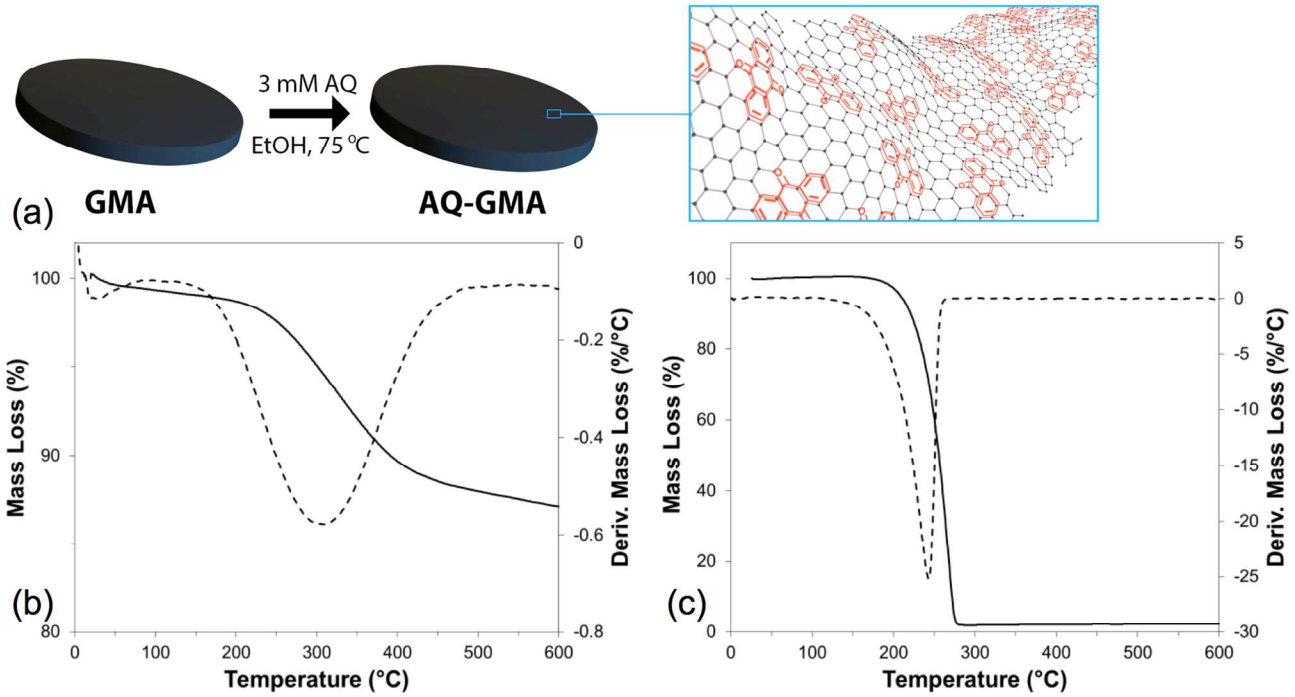

Figure 1: (a) Synthetic procedure and schematic illustration of non-covalent AQ functionalization of GMA electrodes. (b) TGA curve for 250 µm thick AQ-GMA disk with 11.2 wt.% AQ loading (10.1% of total mass) and (c) TGA curve for bulk AQ (Ar flow 10 mL/min, 10 °C/min temperature ramp). Derivative mass loss curves (dashed lines) show peaks at different temperatures for the AQ-GMA vs. bulk AQ. A higher temperature of more than 60 °C indicates adsorption of the AQ molecules on the carbon substrate.

Anthraquinone adsorption onto the GMA electrode produced reversible and stable faradaic charge storage in 1 M HCl aqueous electrolyte, as illustrated by the cyclic voltammagram (CV) in **Figure 2a.** By integrating the area under the AQ redox peak centered at –0.1 V vs. SCE, we determined that each adsorbed AQ molecule stores the expected two electrons, in accordance with the redox mechanism in **Equation 1** (theoretical capacity of AQ: 927 C/g).

(1) 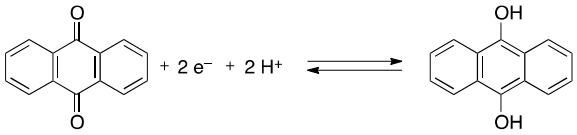

The oxidation and reduction peaks are separated by 60 mV, revealing a small overpotential and thus good energy efficiency. Notably, the baseline double-layer capacitance of the GMA electrode (solid line) is not significantly impacted by non-covalent modification with AQ. The charge storage capacity of AQ adsorbed on GMA remains constant at potential sweep rates up 60 mV/s, at which point the uncompensated solution resistance causes such large overpotential that AQ cannot fully charge within the applied voltage window (**Figure 2b)**. This impressive rate performance is further indication that the AQ molecules are stably attached to the internal surfaces of the porous GMA electrode and that the mechanism is limited by H^+ mass transfer. We also found that we could tune the AQ redox potential by varying electrolyte pH and/or through the addition of supporting electrolytes (**Figure S1**, ESI). In our electrochemical testing we found that 1–1.5 M HCl electrolyte gave the best combination of coulombic efficiency, cycling stability, and rate performance.

The gravimetric capacitance value of 191 F/g for AQ-GMA was derived by integrating the CV curve over the entire voltage range (–0.4 – 0.6 V). Importantly, use of the farad capacitance metric (i.e., coulomb/volt) is accurate only for describing purely capacitive systems where the stored charge increases linearly with applied voltage. The AQ faradaic mechanism instead stores and delivers its charge near –0.1 V vs. SCE and therefore makes the capacitance value highly dependent on the voltage range considered. For example, a gravimetric capacitance value of 540 F/g for AQ-GMA can be derived if the voltage range in question is limited to –0.2 – 0 V vs. SCE. Because the faradic mechanism in AQ-GMA behaves like the active material in a battery, in the following discussion we use the battery metrics C/g (functionally equivalent to mAh/g) or Wh/kg to more accurately describe how AQ functionalization affects device performance.

To assess the energy storage and power performance of AQ-GMA supercapacitor electrodes, we assembled two-electrode cells consisting of 250 µm thick AQ-GMA disks with 10-14 wt.% AQ loading (negative electrode) paired with untreated GMA counter electrodes (UCEs) of various masses but equivalent footprint areas in 1 M HCl aqueous electrolyte. To optimize the overall cell performance (i.e., to provide enough capacity on the counter electrode to fully utilize the capacity of AQ-GMA), we paired a 250 µm thick AQ-GMA with (i) a 250 µm UCE of equal mass, (ii) a 500 µm thick UCE

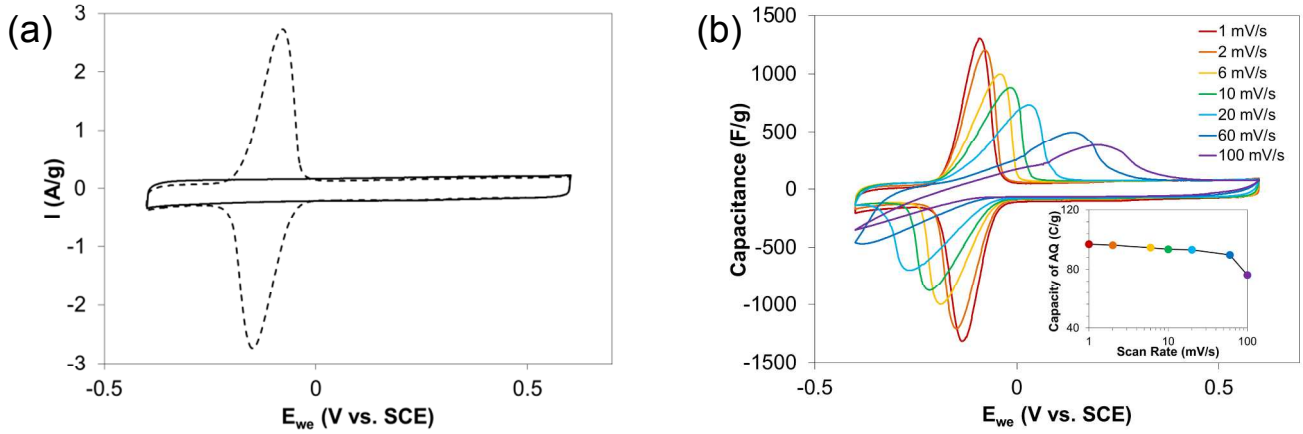

Figure 2: (a) Cyclic voltammagram (2 mV/s, 1 M HCl) for 250 µm thick GMA disks, as prepared (solid line), and with 12.4 wt.% AQ loading (dashed line). (b) CVs of the same 12.4 wt.% AQ-GMA sample at different potential sweep rates. The inset plot illustrates that AQ contribution to charge storage capacity remains constant until >60 mV/s, where solution resistance causes such large overpotentials that AQ cannot fully charge within the applied voltage window. (Capacity values were derived by integrating the discharge peak associated with AQ and subtracting underlying capacity of GMA.)

of 2X mass, and (iii) a 1,000 µm thick UCE of 4X mass. For comparison, we also assembled two-electrode cells consisting of two untreated GMA electrodes of equal mass, as well as two AQ-GMA electrodes of equal mass and AQ loading. The charge-discharge curves for those cells at ~2 A/g are presented in **Figure 3**. The gravimetric charge storage capacity (normalized to GMA mass of working electrode) of AQ-GMA electrodes paired with 250 µm, 500 µm, and 1000 µm UCEs is dramatically increased compared with the untreated GMA electrode (baseline capacity: 59 C/g). Coupling AQ-GMA with a 500 µm UCE gave a 2.6X increase in capacity (156 C/g) over the untreated electrode, with coulombic efficiency >98%.[35] This pair also demonstrated self-discharge behavior comparable to an untreated GMA electrode pair (<20% after 1 min), which suggests that the AQ remains in position on the substrate when charged and does not diffuse away (**Figure S2,** ESI). AQ-GMA paired with a 1,000 µm UCE gave a 2.5X increase in capacity

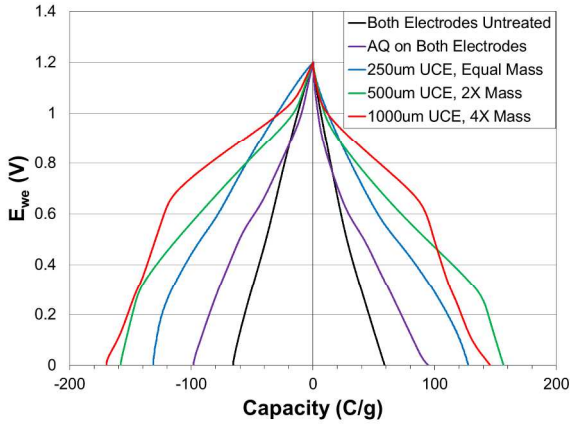

Figure 3: Charge-discharge curves for 250 µm thick AQ-GMAs with 11-14% AQ loading paired with various counter electrodes (UCE = untreated counter electrode) in 1M HCl at ~2 A/g. Curves are normalized to coulombs per gram of GMA working electrode (negative values are charge, positive are discharge).

(145 C/g) over the untreated electrode. Notice, however, that AQ-GMA paired with a 1,000 µm UCE discharged more electrons at a higher voltage, indicating higher energy density for that pair (by ~4% over AQ-GMA/500 µm UCE based on the mass of AQ-GMA). The slight difference in total coulombs stored may be due to minor variations in AQ loading among the AQ-GMA electrodes. Coupling AQ-GMA with a 250 µm UCE resulted in incomplete utilization of the capacity of the AQ (125 C/g). Similarly, the two-electrode cell consisting of AQ-GMA for both the working and counter electrodes showed only a modest increase in storage capacity (94 C/g) compared to the untreated electrodes. The redox charge storage capacity of AQ is biased to the cathodic end of the voltage range (**Figure 2**) and is therefore not expected to be active when used as an anode. These results highlight the importance of pairing AQ-GMA with counter electrodes having appropriate charge storage characteristics to maximize the energy density of the system. Full optimization will require an asymmetric cell design in which AQ-GMA serves as the negative electrode.[23]

The Ragone curves in **Figure 4** illustrate the increased specific energy and power of AQ-GMAs. When the entire mass of both electrodes is considered (**Figure 4a**), AQ-GMAs paired with either 250 µm or 500 µm UCEs perform nearly identically, and have more than double the energy density of unmodified GMAs even at relatively high power. This remarkable result indicates that the AQ faradaic mechanism responds about as fast as the GMA double-layer capacitive mechanism, which is very fast given the high conductivity of the 1 M HCl electrolyte. This extremely fast redox contribution requires intimate contact between AQ and the GMA that serves a current collector. AQ-GMA paired with a 1,000 µm UCE is limited in specific energy and power because the significantly increased mass of the counter electrode decreases the effective serial capacitance. However, when the Ragone curves are instead normalized to the mass of the working electrode (**Figure 4b**), AQ-GMA paired with a 1,000 µm UCE surpasses

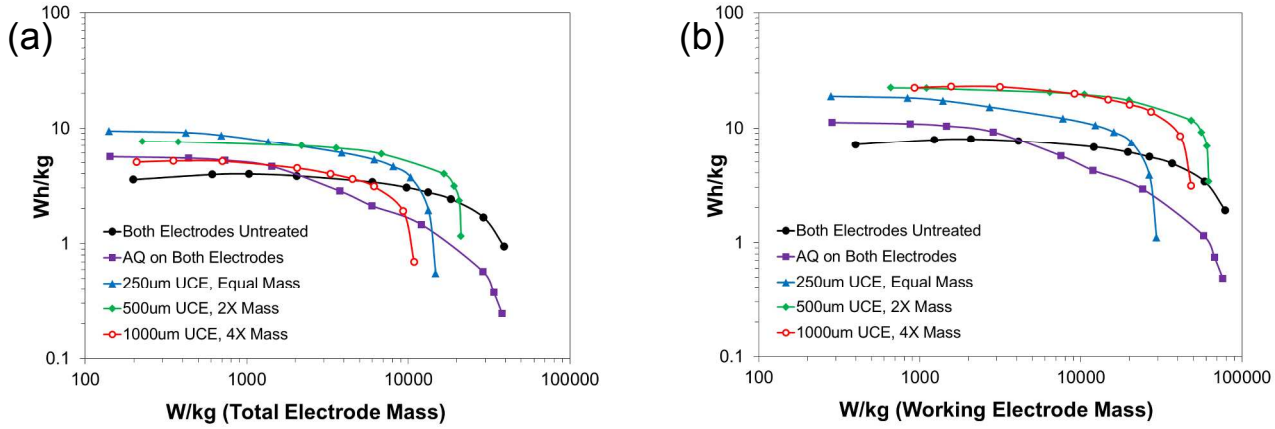

Figure 4: Ragone plot for 250 µm thick AQ-GMAs with 11-14% AQ loading paired with various counter electrodes (UCE = untreated counter electrode), (a) with respect to total electrode mass (working and counter), and (b) with respect to working electrode GMA mass. (For experimental details, see ESI)

the performance of the 250 µm UCE and performs as well as the 500 µm UCE until higher power.

To further increase the volumetric energy density, we tested our recently discovered approach to increase the volumetric energy density of GMA electrodes by increasing the density through mechanical compression, which drastically decreases the volume of inactive "wasted" space in macropores.[11] Our results show that the compression approach can be directly applied to AQ-GMA electrodes. Specifically, we observed an 8-fold increase in volumetric energy density after 8-fold compression while maintaining excellent power performance (**Figure S3** ESI).

Finally, we assessed the long-term stability of AQ-GMA electrodes by performing 10,000 charge-discharge cycles at 10 A/g in a two-electrode cell comprised of a 250 µm thick AQ-GMA with 10 wt.% AQ loading paired with a 500 µm UCE (**Figure S4**, ESI). The AQ-GMA electrode retained over 80% of its original capacity for >9,000 cycles while 77% of its original capacity remained at 10,000 cycles. Interestingly, the energy storage capacity of the AQ-GMA electrode *increased* over the first 500 cycles before beginning a gradual decline. This may be due to a cycling-induced change in local acid concentration within the porous structure of AQ-GMA, as the AQ redox peak shifted to higher potential and thus higher energy while the total coulombs stored did not increase (**Figure S5**, ESI). For comparison, we also subjected an untreated GMA electrode to 10,000 charge-discharge cycles under identical conditions and did not observe an initial increase in capacity. The untreated material maintained 91% of original capacity after 10,000 cycles.

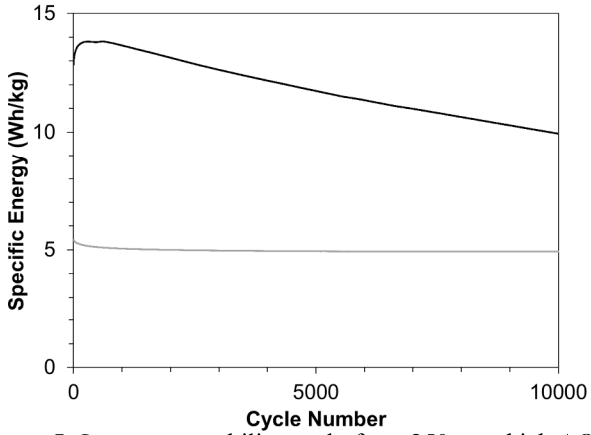

Figure 5: Long-term stability study for a 250 µm thick AQ-GMA electrode with 10 wt.% AQ paired with a 500 µm UCE (black line), and stability of untreated GMA electrode (gray line). Two-electrode cell, 10 A/g, 1 V window, 1.5 M HCl. After 10,000 cycles AQ-GMA maintains 77% of original capacity and stores 2X more energy than the untreated electrode.

The gradual loss of performance of the AQ-GMA electrode could be due in part to the shifting of the AQ redox peak beyond the 1 V potential limit, thus leaving AQ capacity unutilized. Degradation of the GMA electrode due to changing pH conditions could also reduce the ability of AQ to remain adsorbed on the electrode surface. Despite the loss of capacity after 10,000 cycles, the AQ-GMA electrode maintained 2X higher energy storage capacity compared with the untreated electrode (**Figure 5**). Moreover, the stability of AQ-GMAs at high power is especially impressive when compared to typical batteries, which have a service life of 500-2,000 cycles, and surpasses many other pseudocapacitive materials.[36] The stability of our non-covalent functionalization approach is a consequence of the intrinsic stability of the AQ redox system and the low solubility of AQ in aqueous electrolytes.

Theoretical Calculations

In order to compare the measured capacities to the theoretical limits, we performed density-functional theory calculations of AQ adsorbed on a single graphene sheet (representing GMA) using the Quantum-ESPRESSO code (for details, see ESI).[37] For lower computational cost, we examined AQ adsorption at 24.3 wt.% loading (one AQ per 54 graphene carbon atoms, **Figure 6b**). However, in order to more directly compare the system behavior at the more dilute loading densities found in the experiments, we also interpolated the

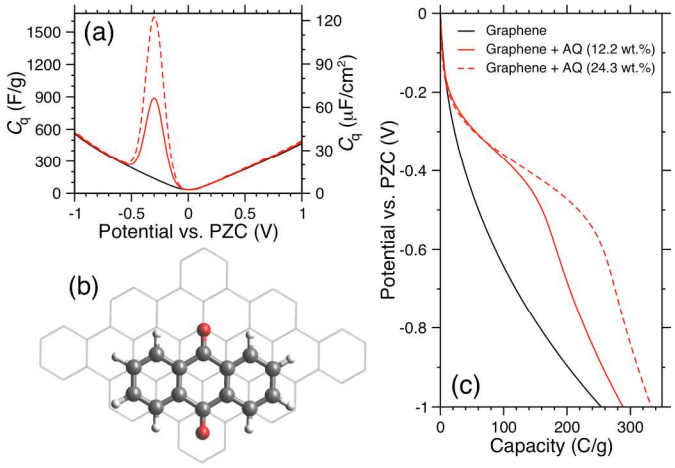

Figure 6: Theoretical differential quantum capacitance of graphene without AQ (black line), with 12.2 wt.% AQ (red solid line), and with 24.3 wt.% AQ (red dashed line). (b) Unit cell used in the 24.3 wt.% AQ calculations (gray=C, white=H, red=O), with the underlying graphene lattice shown in light gray. (c) Ideal charge/discharge curves calculated for each of the configurations. Potentials represent half-cell potentials, referenced to the potential at the point of zero charge (PZC, approximated as the zero-bias Fermi level). The theoretical capacity at a full cell voltage of 1.2 V (i.e., ~–0.6 V in Figure 6c) is 183 C/g for 12.2 wt.% loading, in very good agreement with experimental results. Gravimetric quantities are normalized to the mass of the underlying graphene sheet.

higher-density and pristine graphene results to obtain an estimate for 12.2 wt.% AQ loading.

The results for the differential quantum capacitance are shown in **Figure 6a**. The redox peak corresponding to the AQ is clearly visible at around –0.3 V with respect to the potential of zero charge of the half-cell. This translates to about –0.6 V across a symmetric two-electrode configuration, in excellent agreement with the corresponding features in the cyclic voltammagram (**Figure 2**). Note that the redox peak appears only at negative bias, in agreement with the asymmetric response in the experiments. Moreover, we are able to confirm that the addition of AQ does not affect the background capacitance contribution from the carbon when normalized to the mass of the graphene substrate.

The redox feature also manifests in the integrated total capacity curve (**Figure 6c**), which can be compared directly to the measured quantity in Figure 3. A voltammetric shoulder becomes visible at around –0.4 V for the half-cell, which is approximately –0.8 V across a full cell-equivalent two-electrode setup. Again, this is in excellent agreement with the experimental results. According to the calculations, the theoretical capacity at a full cell voltage of 1.2 V (~–0.6 V in Figure 6) is 183 C/g for 12.2 wt.% loading. We are able to achieve values that are very close to this theoretical maximum with the proper choice of counter electrode (**Figure 3**). This suggests that nearly all of the incorporated AQ is accessible for charge storage. We point out that according to Figure 6c, if AQ loading could be stabilized at ~25 wt.%, then the theoretical capacity would increase further to ~260 C/g at –0.6 V (half cell).

Conclusions

In summary, we have developed an anthraquinone-modified GMA hybrid battery/supercapacitor electrode with 2.9-fold increased electrical energy storage capacity over an untreated GMA electrode. Electrochemical measurements and theoretical calculations show that supercapacitor electrodes fabricated from AQ-GMA materials have high energy and power density, and excellent cycling stability. AQ stores two electrons per 14 carbon atoms (927 C/g or 258 mAh/g), which is comparable to the theoretical ideal stoichiometric limit of LiC_6 for the intercalated graphite anode of Li-ion batteries; the charge rate of AQ-GMA electrodes is limited only by the mass transfer of protons. Thus, we have integrated a battery-like redox component into a system with supercapacitor power performance. Mechanical compression allows us to further increase volumetric energy density. Moreover, the facile non-covalent route employed for modifying these GMA materials opens the door for further tunability. For example, by treating GMA electrodes with quinones that have formal redox potentials close to the anodic limit, we may be able to further increase their capacity and performance in supercapacitor applications.

Acknowledgements

This work was performed under the auspices of the U.S. Department of Energy by Lawrence Livermore National Laboratory under Contract DE-AC52-07NA27344. Funding was provided by the DOE Office of Energy Efficiency and Renewable Energy, and the Lawrence Livermore National Laboratory Directed Research and Development (LDRD) Grant 12-ERD-035.

Notes and references

Lawrence Livermore National Laboratory, 7000 East Ave. L-367, Livermore, CA 94550, USA
E-mail: campbell82@llnl.gov
Electronic Supplementary Information (ESI) available: [Detailed synthetic procedures, theoretical calculations, Figures S1-S4]. See DOI: 10.1039/b000000x/

1. N. Armaroli and V. Balzani, *Energy Environ. Sci.*, 2011, **4**, 3193.
2. P. Simon and Y. Gogotsi, *Nat Mater*, 2008, **7**, 845–854.
3. P. Simon and Y. Gogotsi, *Acc. Chem. Res.*, 2013, **46**, 1094–1103.
4. H. Jiang, P. S. Lee, and C. Li, *Energy Environ. Sci.*, 2013, **6**, 41–53.
5. M. A. Worsley, P. J. Pauzauskie, T. Y. Olson, J. Biener, J. H. Satcher, and T. F. Baumann, *J. Am. Chem. Soc.*, 2010, **132**, 14067–14069.
6. M. A. Worsley, S. O. Kucheyev, H. E. Mason, M. D. Merrill, B. P. Mayer, J. Lewicki, C. A. Valdez, M. E. Suss, M. Stadermann, P. J. Pauzauskie, J. H. Satcher, J. Biener, and T. F. Baumann, *Chem. Commun.*, 2012, **48**, 8428–8430.
7. M. A. Worsley, T. Y. Olson, J. R. I. Lee, T. M. Willey, M. H. Nielsen, S. K. Roberts, P. J. Pauzauskie, J. Biener, J. H. Satcher Jr., and T. F. Baumann, *J. Phys. Chem. Lett.*, 2011, **2**, 921–925.
8. C. Berger, Z. Song, T. Li, X. Li, A. Y. Ogbazghi, R. Feng, Z. Dai, A. N. Marchenkov, E. H. Conrad, P. N. First, and W. A. de Heer, *J. Phys. Chem. B*, 2004, **108**, 19912–19916.
9. S. Das Sarma, S. Adam, E. H. Hwang, and E. Rossi, *Rev. Mod. Phys.*, 2011, **83**, 407–470.
10. B. C. Wood, T. Ogitsu, M. Otani, and J. Biener, *J. Phys. Chem. C*, 2014, **118**, 4–15.
11. M. D. Merrill, E. Montalvo, P. G. Campbell, Y. M. Wang, M.

Stadermann, T. F. Baumann, J. Biener, M. A. Worsley, *RSC Adv.,* 2014*,* DOI: 10.1039/C4RA08114E.
12. X. Zhao, B. M. Sánchez, P. J. Dobson, and P. S. Grant, *Nanoscale*, 2011, **3**, 839.
13. R. Liu, J. Duay, and S. B. Lee, *Chem. Commun.*, 2011, **47**, 1384–1404.
14. J. Jiang, Y. Li, J. Liu, X. Huang, C. Yuan, and X. W. D. Lou, *Adv. Mater.*, 2012, **24**, 5166–5180.
15. H. Jiang, J. Ma, and C. Li, *Adv. Mater.*, 2012, **24**, 4197–4202.
16. A. E. Fischer, K. A. Pettigrew, D. R. Rolison, R. M. Stroud, and J. W. Long, *Nano Lett.*, 2007, **7**, 281–286.
17. X. Dong, W. Shen, J. Gu, L. Xiong, Y. Zhu, H. Li, and J. Shi, *J. Phys. Chem. B*, 2006, **110**, 6015–6019.
18. M. Sathiya, A. S. Prakash, K. Ramesha, J.-M. Tarascon, and A. K. Shukla, *J. Am. Chem. Soc.*, 2011, **133**, 16291–16299.
19. X. Wang, G. Li, Z. Chen, V. Augustyn, X. Ma, G. Wang, B. Dunn, and Y. Lu, *Adv. Energy Mater.*, 2011, **1**, 1089–1093.
20. M. Quan, D. Sanchez, M. F. Wasylkiw, and D. K. Smith, *J. Am. Chem. Soc.*, 2007, **129**, 12847–12856.
21. K. Kalinathan, D. P. DesRoches, X. Liu, and P. G. Pickup, *J. Power Sources*, 2008, **181**, 182–185.
22. Z. Algharaibeh, X. Liu, and P. G. Pickup, *J. Power Sources*, 2009, **187**, 640–643.
23. Z. Algharaibeh and P. G. Pickup, *Electrochemistry Communications*, 2011, **13**, 147–149.
24. Q. Wu, Y. Sun, H. Bai, and G. Shi, *Phys. Chem. Chem. Phys.*, 2011, **13**, 11193.
25. G. Pognon, T. Brousse, L. Demarconnay, and D. Bélanger, *J. Power Sources*, 2011, **196**, 4117–4122.
26. M. Weissmann, O. Crosnier, T. Brousse, and D. Bélanger, *Electrochimica Acta*, 2012, **82**, 250–256.
27. S. Roldán, C. Blanco, M. Granda, R. Menéndez, and R. Santamaría, *Angew. Chem. Int. Ed.*, 2011, **50**, 1699–1701.
28. H. Wang, H. Wu, Y. Chang, Y. Chen, and Z. Hu, *Chin. Sci. Bull.*, 2011, **56**, 2092–2097.
29. D. M. Anjos, J. K. McDonough, E. Perre, G. M. Brown, S. H. Overbury, Y. Gogotsi, and V. Presser, *Nano Energy*, 2013, **2**, 702–712.
30. D. M. Anjos, A. I. Kolesnikov, Z. Wu, Y. Cai, M. Neurock, G. M. Brown, and S. H. Overbury, *Carbon*, 2013, **52**, 150–157.
31. X. Chen, H. Wang, H. Yi, X. Wang, X. Yan, and Z. Guo, *J. Phys. Chem. C*, 2014, **118**, 8262–8270.
32. S. M. Chathoth, D. M. Anjos, E. Mamontov, G. M. Brown, and S. H. Overbury, *J. Phys. Chem. B*, 2012, **116**, 7291–7295.
33. S. O. Kucheyev, J. Biener, T. F. Baumann, Y. M. Wang, A. V. Hamza, Z. Li, D. K. Lee, and R. G. Gordon, *Langmuir*, 2008, **24**, 943–948.
34. W. S. Horton, *J. Phys. Chem.,* 1964, **68**, 2278–2281.
35. Columbic inefficiencies are due to experimental factors (e.g., leaky cells) and are not caused by material itself, as indicated by the >98% efficiency achieved under ideal conditions. Columbic efficiencies for each cell in Figure 3: both electrodes untreated = 89%; AQ on both – 93%; 250 µm UCE – 96%; 500 µu UCE – 98%; 1000 µm UCE – 85%
36. Y. Zhang, H. Feng, X. Wu, L. Wang, A. Zhang, T. Xia, H. Dong, X. Li, and L. Zhang, *Int. J. Hydrogen Energy*, 2009, **34**, 4889–4899.
37. P. Giannozzi, S. Baroni, N. Bonini, M. Calandra, R. Car, C. Cavazzoni, D. Ceresoli, G. L. Chiarotti, M. Cococcioni, I. Dabo, A. Dal Corso, S. de Gironcoli, S. Fabris, G. Fratesi, R. Gebauer, U. Gerstmann, C. Gougoussis, A. Kokalj, M. Lazzeri, L. Martin-Samos, N. Marzari, F. Mauri, R. Mazzarello, S. Paolini, A. Pasquarello, L. Paulatto, C. Sbraccia, S. Scandolo, G. Sclauzero, A. P. Seitsonen, A. Smogunov, P. Umari, and R. M. Wentzcovitch, *J. Phys.: Condens. Matter*, 2009, **21**, 395502.